

Design of a Single-Layer C/X Dual-Band Reflectarray Antenna with Low Cross-Polarization

Li Liu, Yufeng Liu*, Zhiyuan Yang, and Liping Han

School of Physics and Electronic Engineering, Shanxi University, Taiyuan 030006, China

ABSTRACT: A single-layer reflectarray antenna working at C- and X-bands is designed in this paper. The proposed reflectarray element is mainly composed of three square rings. Four phase delay lines are attached to the outer ring to obtain the phase shift at C-band, and the inner two square rings are utilized to extend the phase range at X-band. The phase shift of the element reaches up to 375° and 560° at 5.9 GHz and 10.4 GHz, respectively. The cross-polarization level of the reflectarray is effectively suppressed by using a mirror symmetric element arrangement. To experimentally validate the proposed design, a center-fed dual-band prototype reflectarray with the size of $180\text{ mm} \times 180\text{ mm}$ is designed, fabricated, and tested. The measured peak gains are 16.5 dBi at 6.2 GHz and 17.1 dBi at 10.3 GHz, respectively. Besides, the measured 1-dB gain bandwidth is 9.15% (5.83–6.37 GHz) at the lower band and 3.27% (10.12–10.46 GHz) at the upper band, respectively. Moreover, the cross polarizations at both bands are under -21 dB .

keywords: Reflectarray antenna, dual-band, single layer, low cross-polarization

1. INTRODUCTION

Recently, reflectarray antenna has drawn much attention since it combines several advantages of both parabolic reflector antennas and planar arrays such as light weight, compact size, easy fabrication, and low cost [1–4]. A reflectarray antenna is mainly composed of a feed antenna, a bottom reflector, and an array of elements with specific sizes to compensate for spatial phase delays and then to form a planar wavefront over the aperture [5].

To meet the requirement of the dual-band directive antenna in modern telecommunication systems: satellite communications, remote sensing, etc., dual-band operation has become an important research area in reflectarray antenna design. In the past decades, there are mainly two techniques to realize dual-band reflectarray antennas. One technique is to employ a double-layer configuration [6–11]. Although the frequency selective surface (FSS)-backed upper layer is nearly transparent to the lower layer, its blockage effect is inevitable. Moreover, the overall profile of the antenna is also doubled. The other is to implement dual-band elements on a single-layer substrate [12–15]. This technique not only possesses the low-profile advantage of the traditional reflectarray antenna but also eliminates the shielding effect. However, it leads to closer element spacing and smaller phase variation.

In this paper, a single-layer C/X dual-band reflectarray antenna is proposed. The proposed dual-band element consists of double square rings operating in the X band and a larger square ring attached with four phase-delay lines operating in the C band. Two different structures are arranged in a single element. The mutual coupling of this element configuration can be taken into account in the element analysis. A dual-band slot-

loaded microstrip patch antenna is utilized as the feed source. To effectively reduce the cross-polarization levels of the proposed reflectarray antenna, a mirror-symmetrical arrangement for elements has been adopted.

This paper is organized as follows. Section 2 introduces the structure of the element and the process of analyzing the reflection phase. Section 3 presents the design of the feed antenna and reflectarray. Section 4 gives the results of measurement and simulation and discusses these results. Section 5 is the conclusion of the whole work.

2. DUAL-BAND ELEMENT DESIGN AND ANALYSIS

2.1. Element Configuration

The configuration of the proposed dual-band element is shown in Figs. 1(a) and (b). The element is composed of triple square rings and four attached phase-delay lines. In the X-band, the internal square loop operates, while the outer square loop, augmented with phase delay lines, functions in the C-band. The element is arranged in a square lattice with a period of $P = 16\text{ mm}$, which corresponds to $0.31\lambda_0$ at 5.9 GHz and $0.55\lambda_0$ at 10.4 GHz. The element is etched on a substrate with a thickness of $h = 2\text{ mm}$ and a relative permittivity of $\epsilon_r = 2.65$. The metal ground is etched on the bottom surface of the same lower substrate. The two substrates are separated by an air layer of h_1 , which makes the reflection phase curve more linear and broaden the phase shift range.

At low frequencies, the phase shift can be controlled by adjusting the length of the four delay lines connected to a square ring with a length of L . It is noteworthy that the phase delay line is partitioned into two distinct parts, c and c_1 , respectively. The width of the square ring and the interconnecting delay line

* Corresponding author: Yufeng Liu (liuyufeng@sxu.edu.cn).

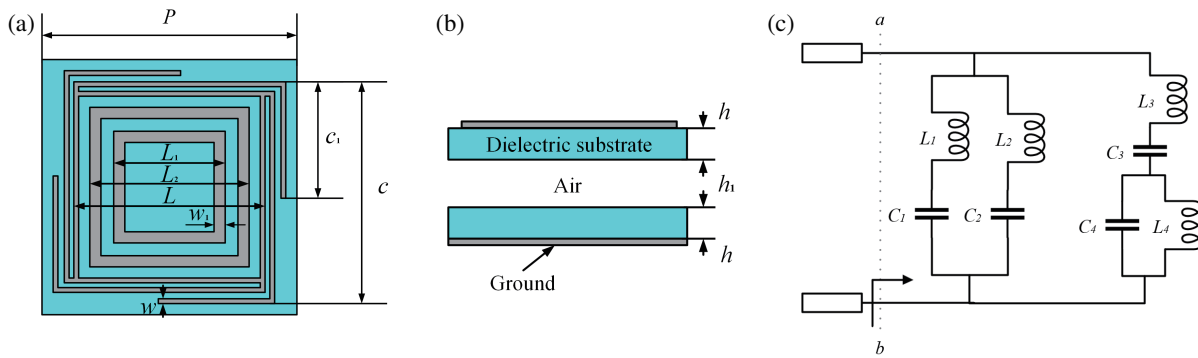


FIGURE 1. Geometry of the proposed unit cell: (a) top view of the unit (b) side view of the unit and (c) equivalent circuit diagram of the unit.

TABLE 1. Design parameters of the proposed element.

Parameters	P	h	h_1	w	L
Values (mm)	16	2	5	0.3	12

TABLE 2. Optimal parameters of the element.

Parameters	a	b	Y_f
Values (mm)	13.3	12.25	2
Parameters	sh	sl	sw
Values (mm)	5.46	11	0.19

is denoted as w . At high frequencies, the width w_1 of the inner double ring varies proportionally with the side length L_1 of the innermost square ring, with a proportionality factor k , denoted as $w_1 = k \cdot a_1$. Additionally, the side length L_2 of the larger square ring also varies proportionally y with a factor represented by $a_2 = k_1 \cdot a_1$. By altering the length of the square ring L_1 , it is possible to simultaneously adjust the width of the high-frequency double ring and the length of the double square ring, thereby manipulating the phase shift at high frequencies. Fig. 1(c) presents the equivalent circuit model of the dual-frequency unit. When electromagnetic waves impinge on the unit surface, in the low-frequency range, the outer single ring can be equivalent to a series resonant circuit and a parallel resonant circuit in series. In this series connection, the L_3C_3 branch represents a phase delay line, while the L_4C_4 branch represents the characteristics of the outer ring. In the high-frequency range, the double-sided ring can be equivalent to the parallel connection of two series resonant circuits represented by the L_1C_1 branch and the L_2C_2 branch. According to circuit theory, it can be demonstrated that there are two resonant frequencies:

$$f_{low} = \frac{1}{2\pi} \sqrt{\frac{1}{(L_3 + L_4) \cdot (C_3 + C_4)}} \quad (1)$$

$$f_{high} = \frac{1}{2\pi} \sqrt{\frac{1}{(L_1 + L_2) \cdot \left(\frac{1}{C_1} + \frac{1}{C_2}\right)}} \quad (2)$$

2.2. Element Performance

The element's performance is evaluated through the utilization of four surrounding walls with periodic boundary conditions and a Floquet port excitation by conducting full-wave simulations on the CST Microwave Studio platform. Various essential

geometric parameters that affect the element's performance are analyzed and optimized.

The reflection phase curves of the element are at the lower frequency band when the length $c + c_1$ of the phase delay line changes, as illustrated in Fig. 2. The investigation reveals that the phase shift range decreases as L increases. Conversely, a smaller L results in a deterioration of the linearity of the curve. Consequently, the optimal balance between linearity and smoothness of the reflection phase curve is achieved when $L = 12$ mm.

As depicted in Fig. 3, the reflection phase curves of the element exhibit changes when the length of the innermost square ring L_1 is modified at higher frequency bands. It is apparent from the results that changing the values of k and k_1 has a minimal impact on the phase shift, which is primarily observed in the L_1 range of 6–10 mm. Additionally, k_1 has a more significant impact on the phase shift compared to k , with the phase shift showing more linear characteristics when $k = 0.08$ and $k_1 = 0.75$.

The reflection phase curve of the element is investigated for varying values of the air layer thickness, h_1 , at two frequency bands, and the results are presented in Fig. 4. The analysis shows that the effect of h_1 on the phase shift is marginal at the lower frequency band, as depicted in Fig. 4(a). However, at the higher frequency band, h_1 has a significant impact on the phase shift, as illustrated in Fig. 4(b). The phase shift range increases as h_1 decreases, but the reflection phase shift curve becomes steeper. Therefore, $h_1 = 5$ mm is determined to be a suitable compromise.

Table 1 lists the final optimized parameters of the proposed element while Fig. 5 shows the corresponding reflection coefficient curves at two frequency bands. At the lower frequency band, Fig. 5(a) demonstrates that the element achieves a phase shift range of 375° with the phase delay line $c + c_1$ varying from 0 to 27 mm. On the other hand, Fig. 5(b) shows that at the higher frequency band, when the length of the inner ring changes from

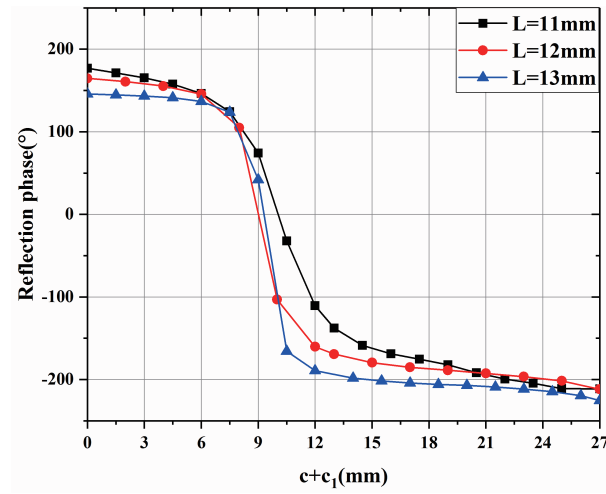


FIGURE 2. Reflection phase curves at C-band for different L .

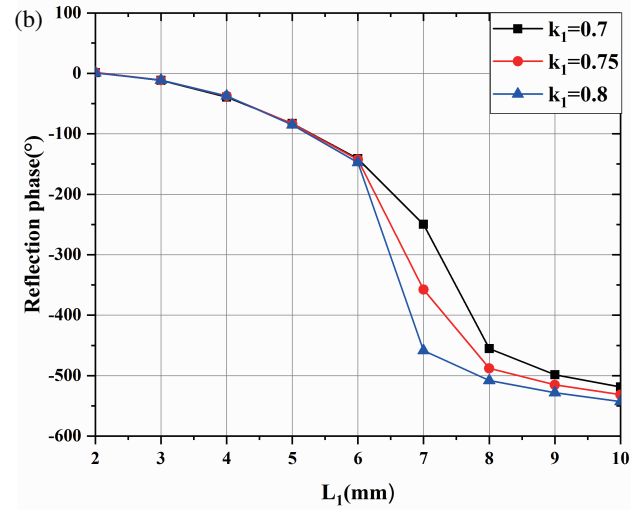
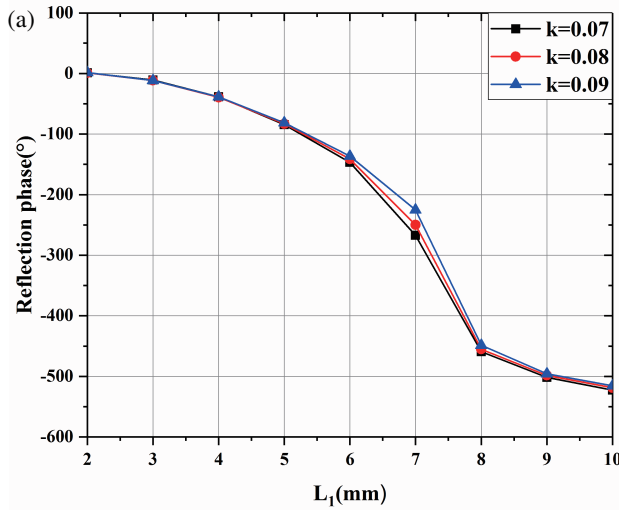


FIGURE 3. Reflection phase curves at X-band: (a) for different values of k and (b) for different values of k_1 .

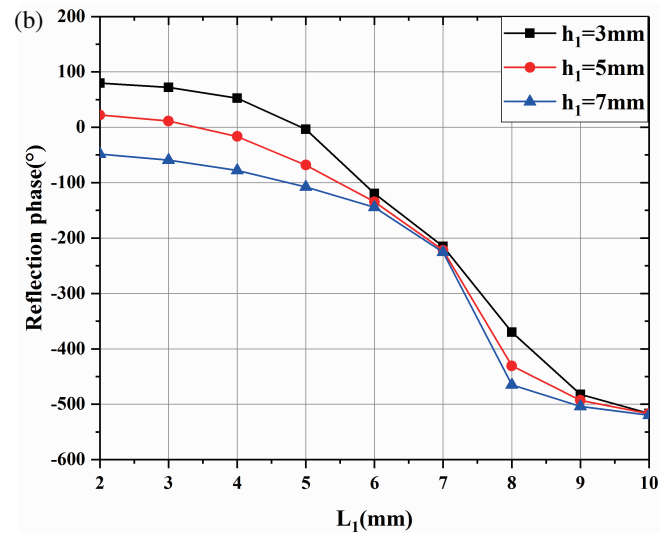
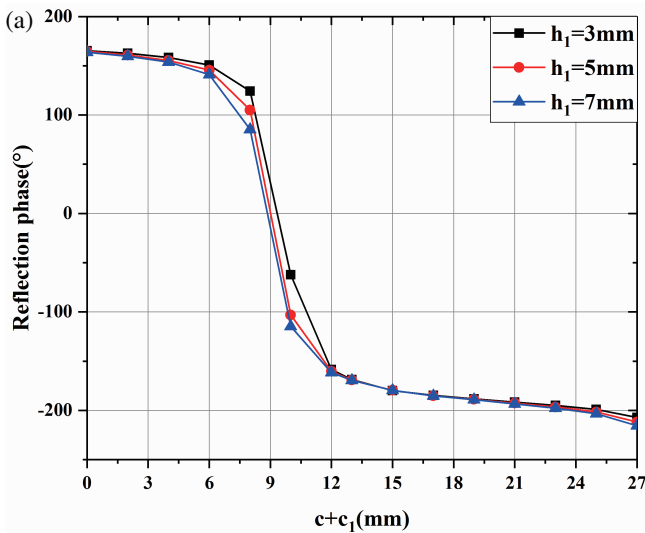


FIGURE 4. Reflection phase curves at two frequency bands for different h_1 : (a) C-band and (b) X-band.

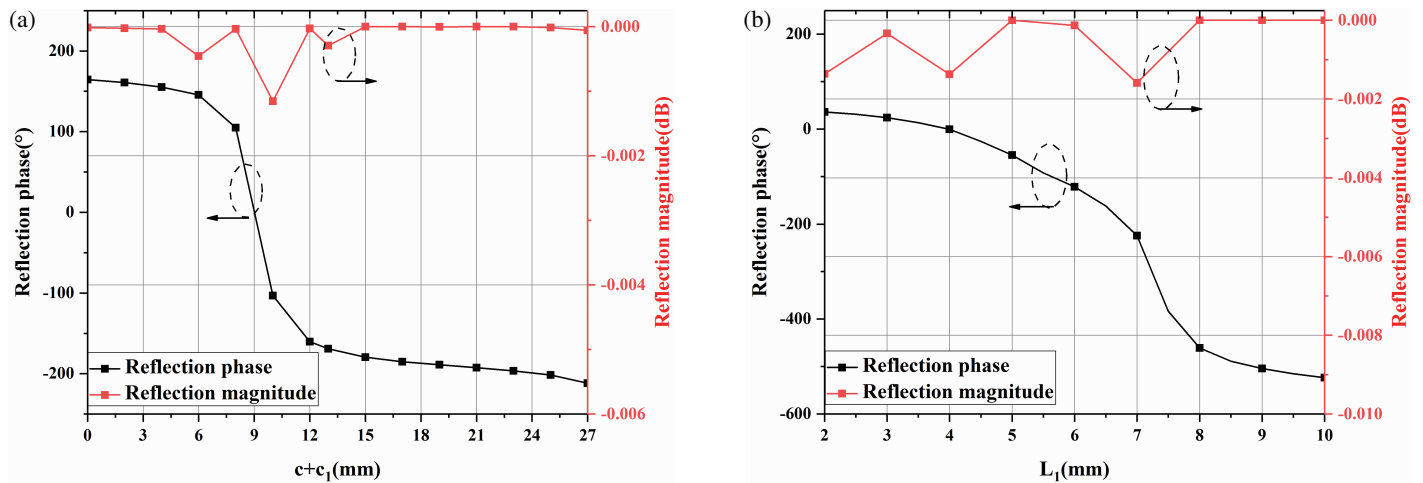


FIGURE 5. Simulation reflection magnitude and phase responses of the element: (a) C-band and (b) X-band.

TABLE 3. Comparison of the performance with previous works on dual-band reflectarray antenna.

Reference	This work	[8]	[12]	[13]	[14]	[15]	[16]
Center Frequency (GHz)	5.9/10.4	20.4/30.2	6.2/9.3	18.95/28.5	20.4/30.2	11.4/13.2	3.5/25.8
Frequency Ratio	1.76	1.5	1.5	1.5	1.5	1.16	7.4
Polarization	Linear	Circular	Circular	Circular	Circular	Linear	Linear
Phase Shift Range	375°/560°	304°/331°	360°/360°	360°/360°	304°/331°		320°/310°
−10 dB impedance bandwidth (%)	2.88%/2.98%	-	-			2%/3%	
unit cell size (mm)	9	9.88	2362	1.575	9.88	7.7	4.624
aperture size (mm)	180 Square	400 Circular	345, Square	19, Square	400 Circular	69.3, Circular	136, Square
F/D	0.44	0.9	0.74/0.87	0.87	0.9		0.59
1-dB gain bandwidth (GHz)	9.15%/3.27%	10.1%/7.2%		16.7%/12.4%	10.1%/7.2%		12.2%/5.8%
aperture efficiencies	22.86%/7.9%	64.1%/65.4%	51.8%/42%	35.1%/46.8%	64.1%/65.4%		74%/34%

2 to 10 mm, a phase shift range of 560° can be obtained. The corresponding reflection magnitudes in dual bands are less than −0.02 dB which satisfies the basic requirements of element design.

Figure 6 illustrates the reflection phase curves of the element for different frequencies. It is observed that the phase curves are nearly parallel for the adjacent frequencies, resulting in good bandwidth performance in both frequency bands.

The mutual coupling interferences between dual-band elements are analyzed. Fig. 7(a) shows that the phase shift curves at the lower frequency band remain nearly invariant when L_1 changes. The reflection phase curves at the higher frequency band with different $c + c_1$ are shown in Fig. 7(b), indicating that the delay line length has a small impact on the phase shift of the higher frequency band. The results demonstrate that the mutual coupling between the two elements is acceptable.

The simulation reflection phase responses of the element under different oblique incidence angles are investigated in both

frequency bands, as shown in Fig. 8. The results indicate that the sensitivity of the element remains constant as the incident angles increase in the lower frequency band. On the other hand, in the higher frequency band, the phase curves display minor variations within 40° until the incidence angle reaches up to 45°.

3. DRAL-BAND REFLECTARRAY ANTENNA DESING

3.1. Feed Antenna Design

As shown in Fig. 9, a dual-band slotted rectangular-patch antenna is utilized as the feed source. The patch incorporates two symmetrical narrow slots with dimensions sl and sw , which are etched on the patch near and parallel to the radiating edges. The distance between the slot and the center is sh , and the feed point is offset from the center along the y -axis by Y_f . To meet the dual-band design requirements of the proposed reflectarray antenna, the center frequencies of the feed antenna are set to

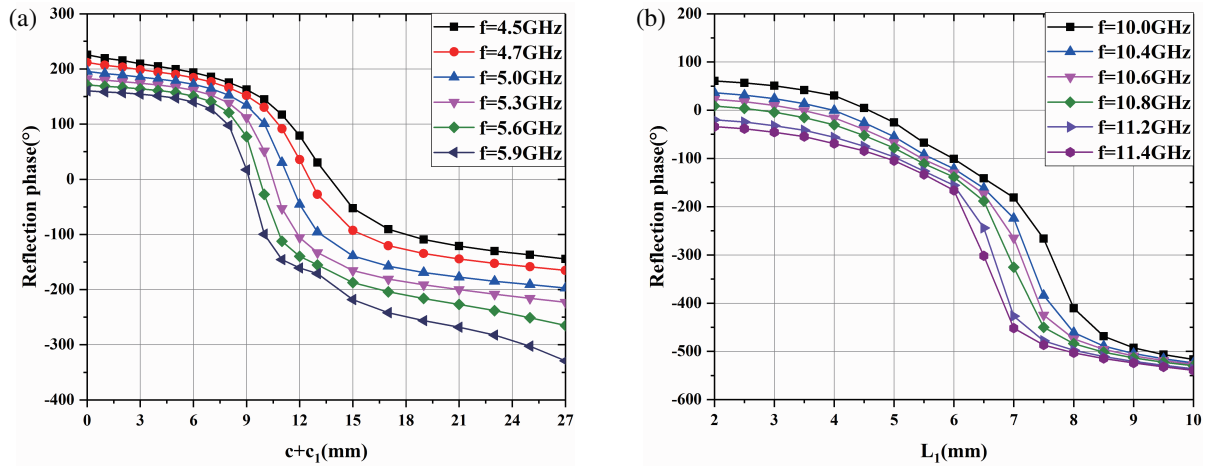


FIGURE 6. Simulation reflection phase curves of the element for different frequencies: (a) C-band and (b) X-band.

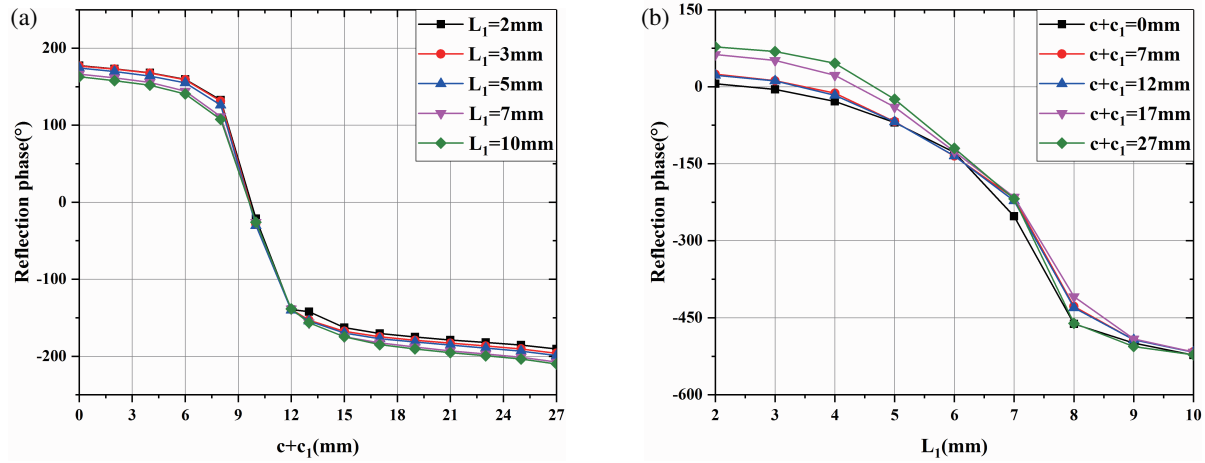


FIGURE 7. Mutual coupling interferences between dual-band elements: (a) C-band and (b) X-band.

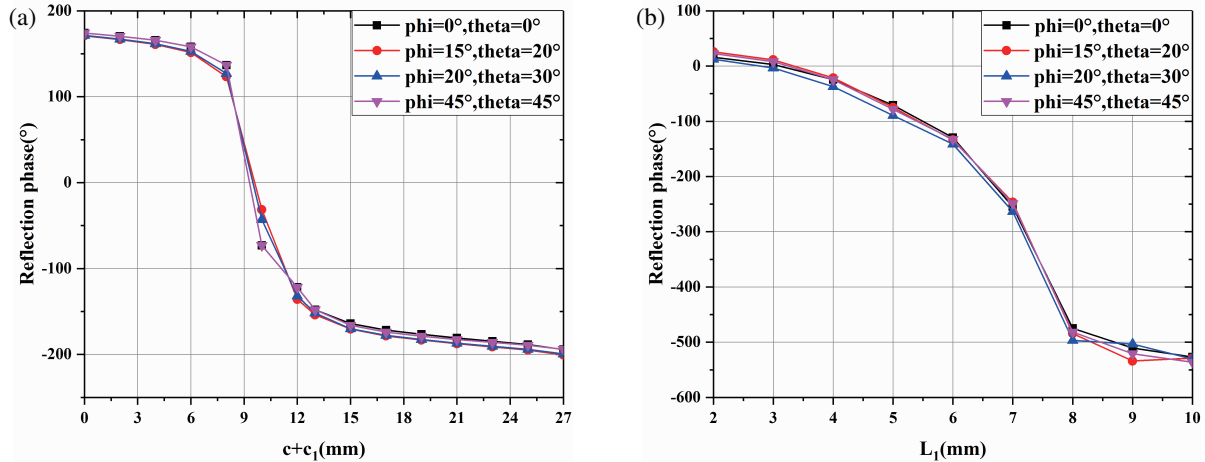


FIGURE 8. Simulation reflection phase shift of the element at different oblique incidence angles: (a) C-band and (b) X-band.

5.9 GHz and 10.4 GHz, with the optimal parameters listed in Table 2.

The measured and simulated reflection coefficient curves are presented in Fig. 10, which indicate a dual-band radiation char-

acteristic, with a value of less than -10 dB observed within the frequency ranges of 5.82 to 6.03 GHz and 10.28 to 10.50 GHz. Fig. 11 displays the radiation pattern of the feeding antenna in the E -plane and H -plane at 5.9 GHz and 10.4 GHz, respec-

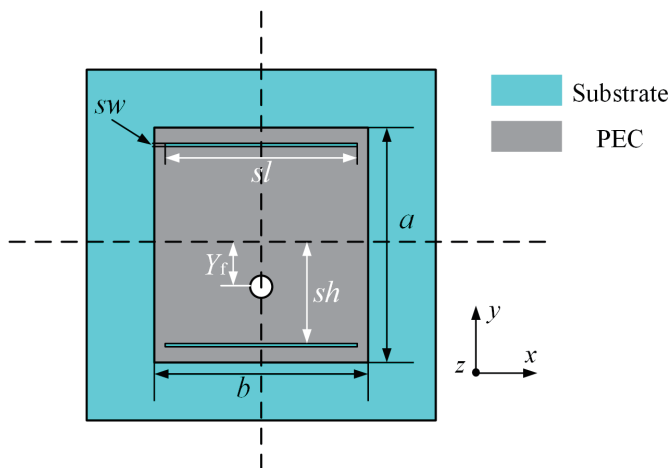


FIGURE 9. Geometry of dual-band feed antenna.

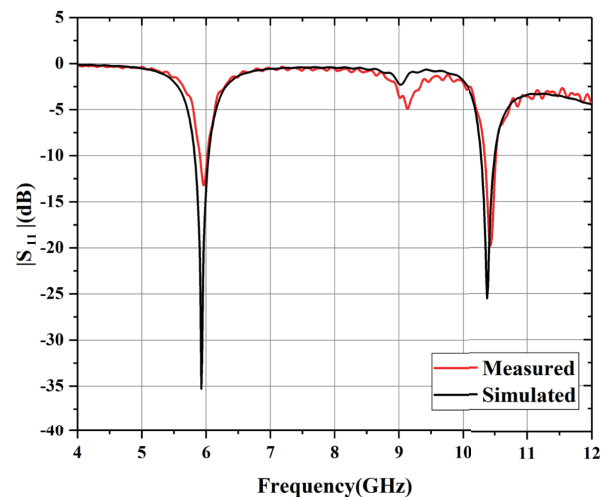


FIGURE 10. Measured and simulated reflection coefficient curves of the feed antenna.

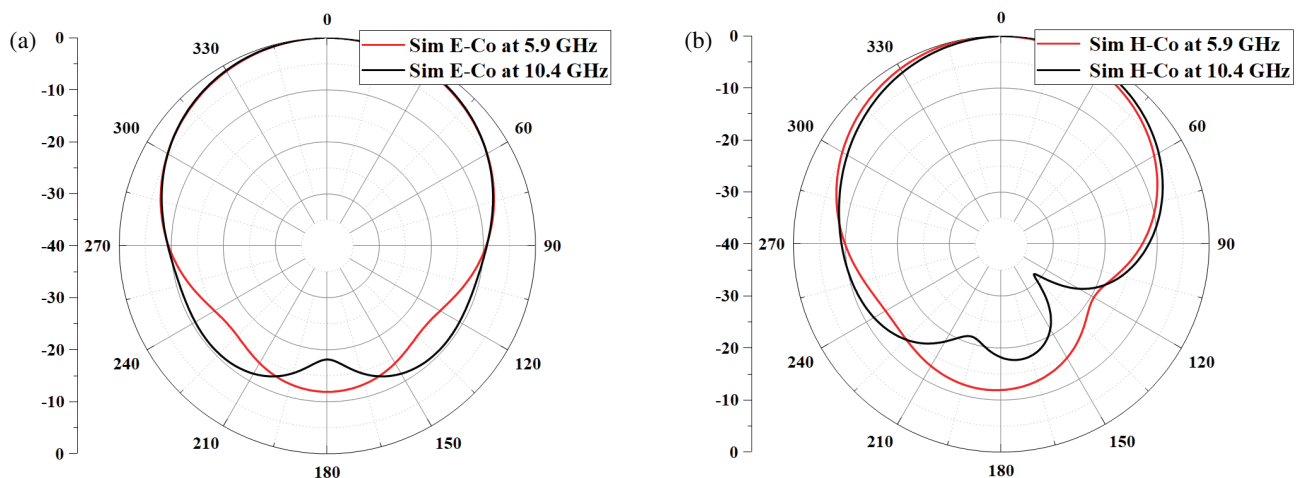


FIGURE 11. Measured radiation patterns at 5.9 GHz and 10.4 GHz. (a) *E*-plane and (b) *H*-plane.

tively. They appear to be nearly rotationally symmetric. These features make the patch antenna a suitable candidate for dual-band reflectarrays.

3.2. Reflectarray Antenna Design

Utilizing the commercial software CST for modeling, we employed classical theory to design a microstrip reflectarray antenna. Calculations were performed using a time-domain solver. To achieve a tilt in the main beam towards the direction (θ_b, ϕ_b) , the reflection phase for each unit can be determined as follows:

$$\phi_R(x_i, y_i) = k_0 (d_i - (x_i \cos \phi_b + y_i \sin \phi_b) \sin \theta_b) \quad (3)$$

$$d_i = \sqrt{(x_i - x_f)^2 + (y_i - y_f)^2 + (z_i - z_f)^2} \quad (4)$$

When the direction of the main beam is perpendicular to the reflector aperture surface (along the z -axis), Equation (3) can

be simplified as follows:

$$\phi_R(x_i, y_i) = k_0 d_i \quad (5)$$

where k_0 is the vacuum propagation constant, and (x_i, y_i) represent the coordinates of the i_{th} element. $\phi_R(x_i, y_i)$ denotes the required phase shift for the i_{th} element. d_i is the distance from the i_{th} element to the phase center of the feed antenna. (x_i, y_i, z_i) represents the position of the feeding source antenna.

The dimensions of the reflective surface for designing a reflectarray are determined based on the following principles. Firstly, the larger the dimensions, the higher the gain of the antenna. However, when the size of the reflectarray is too large, the edge of the reflective surface receives very little energy, resulting in a small contribution to the antenna gain and a decrease in aperture efficiency. It is worth noting that the ratio of focal length to diameter (F/D) has a significant impact on the spillover and illumination efficiency of the reflectarray antenna. A larger F/D ratio makes it easier for the reflectarray antenna to achieve uniform aperture illumination, but as the F/D

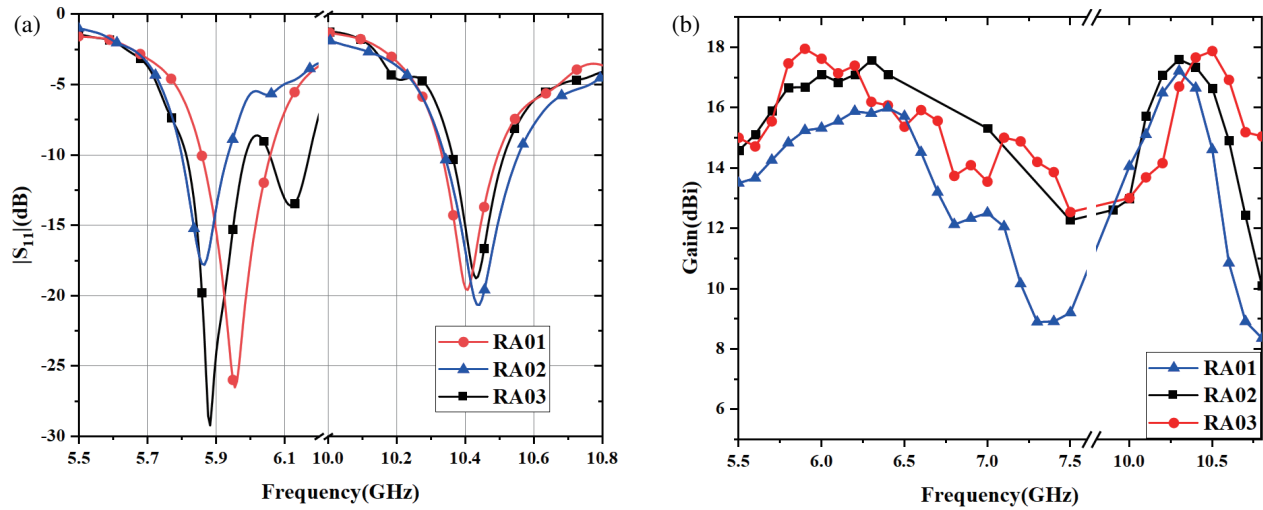


FIGURE 12. Measured reflection coefficient versus frequency and gain with different RAs. (a) Reflection coefficients. (b) Gains.

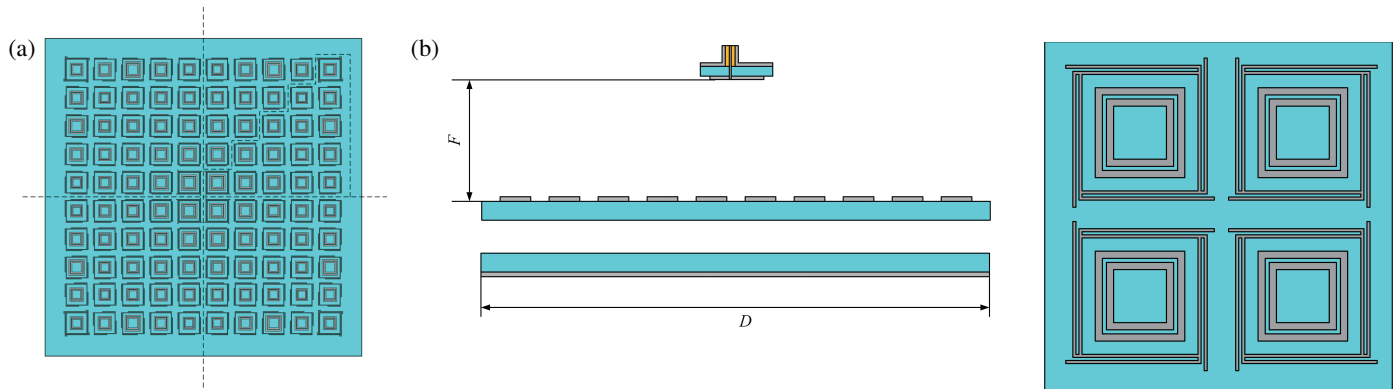


FIGURE 13. Configuration of proposed reflectarray antenna: (a) top view of the antenna and (b) side view of the antenna.

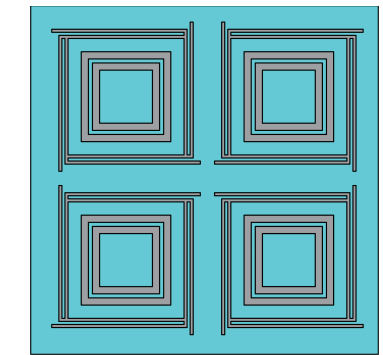


FIGURE 14. Mirror symmetrical arrangement.

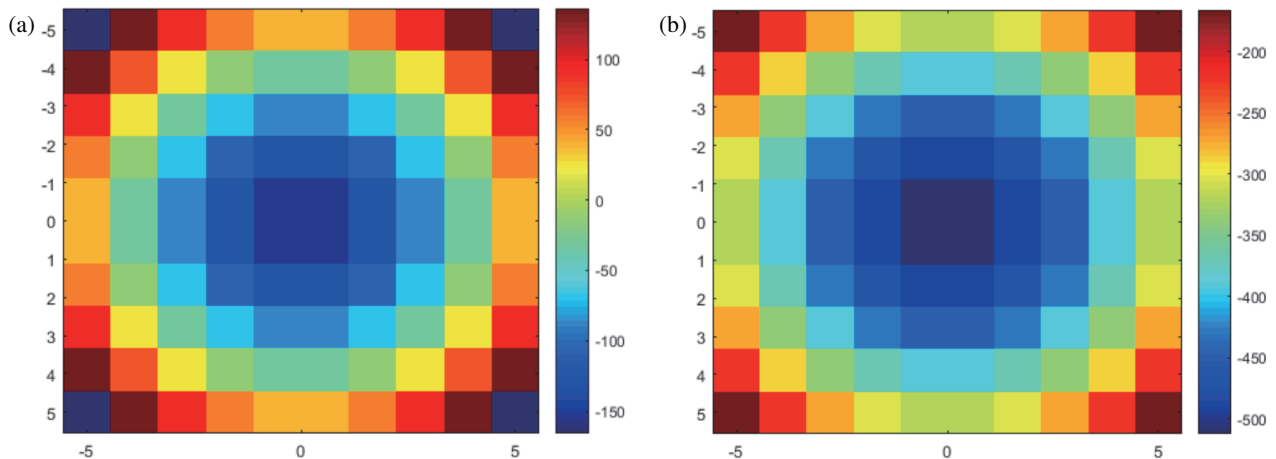


FIGURE 15. Phase distribution of the array aperture. (a) at 5.9 GHz (b) at 10.4 GHz.

ratio increases, the reflectarray cannot intercept a larger portion of the energy. To minimize spillover losses, the height of the feed source must be limited to ensure that the reflector plane covers the main lobe of the feed antenna. Therefore, the reflectarray must have a moderate size to achieve high gain and

high aperture efficiency for the antenna. Then, three reflectarrays, named RA01, RA02, and RA03, were constructed using 9×9 , 10×10 , and 11×11 original unit cells, respectively. Through calculations, it was found that the aperture efficiency

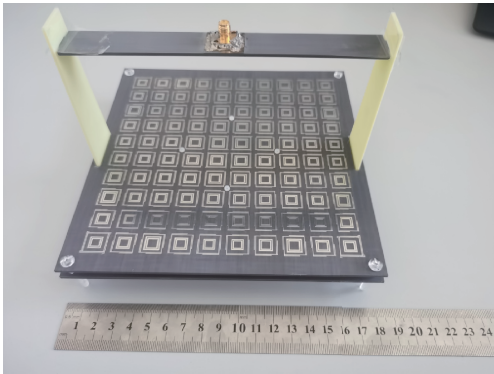


FIGURE 16. Photograph of the fabricated antenna.

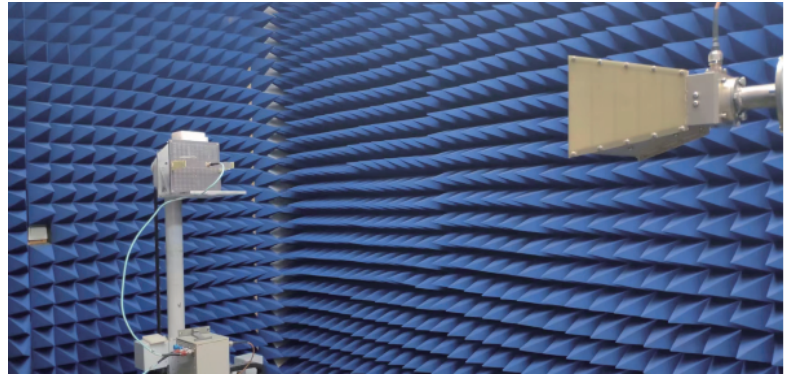


FIGURE 17. Measurement environment.

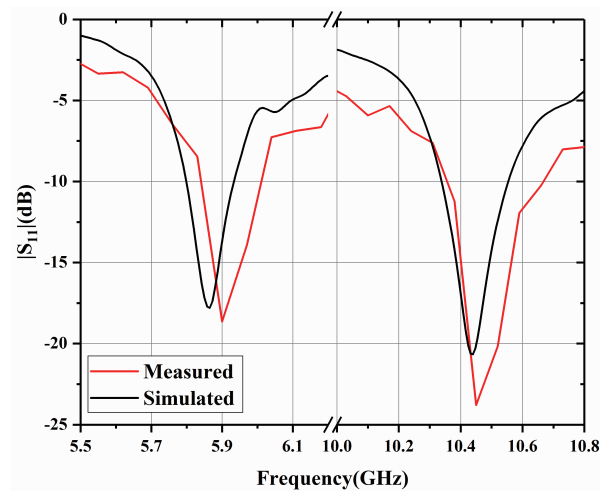


FIGURE 18. Measured and simulated reflection coefficient versus frequency.

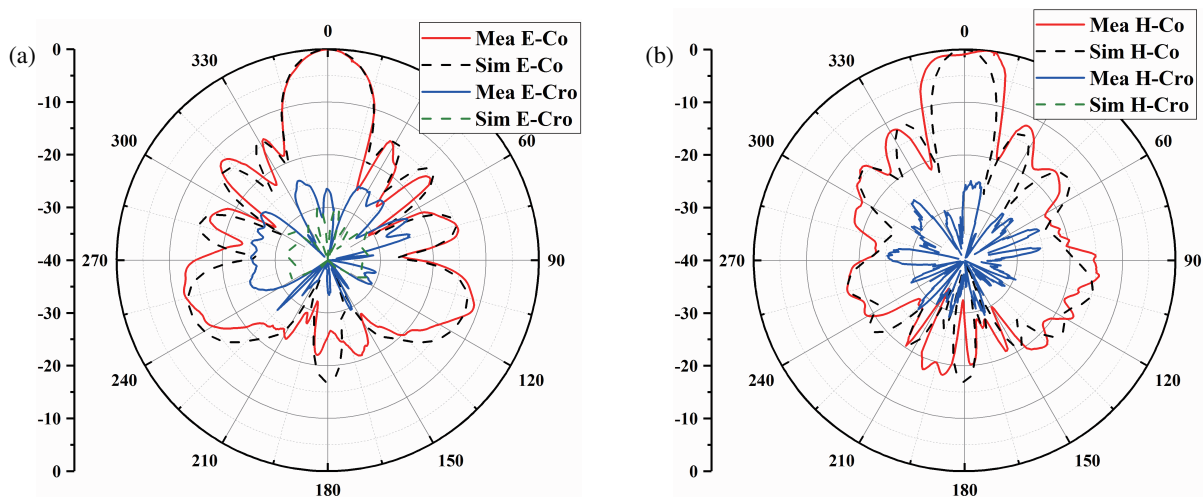


FIGURE 19. Measured and simulated radiation patterns: (a) *E*-plane at 5.9 GHz and (b) *H*-plane at 5.9 GHz.

can be maximized when the *F/D* ratio is 0.44. The three antennas were simulated, and the simulation results were compared.

The simulated gains of the three antennas are shown in Fig. 12. The maximum gains of these antennas are 16.0/17.2, 17.1/17.6, and 17.8/17.9 dBi, respectively. The aperture effi-

ciencies are 21.96%/7.28%, 22.86%/7.9%, and 20.92%/6.73%, respectively. It is apparent that although RA03 has a higher gain than RA02, its aperture efficiency is lower. Considering both gain and aperture efficiency, a 10x10 unit cell reflectarray antenna operating at 5.9 and 10.4 GHz was designed.

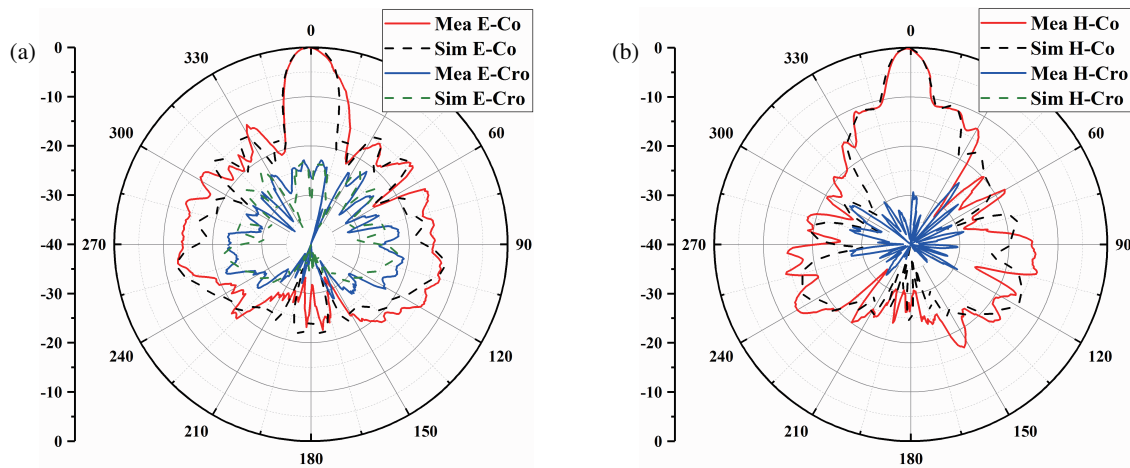


FIGURE 20. Measured and simulated radiation patterns: (a) *E*-plane at 10.4 GHz and (b) *H*-plane at 10.4 GHz.

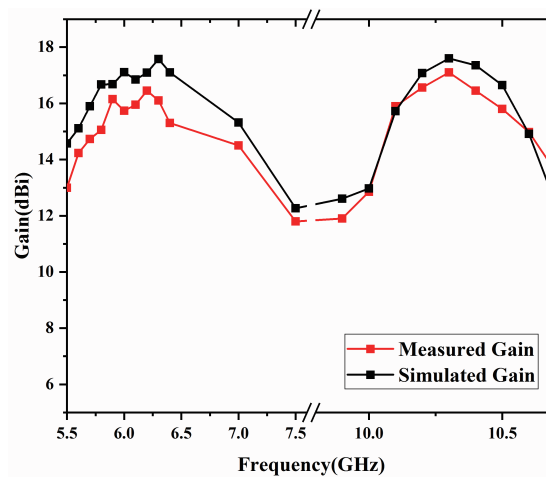


FIGURE 21. Measured and simulated gain of the proposed antenna.

To accommodate the support structure, the size of the reflectarray was increased to $180 \times 180 \text{ mm}^2$, as shown in Fig. 13. The selection of an appropriate element arrangement is crucial in reducing the cross-polarization of the far field. In this research, we adopted a mirrored arrangement of elements between adjacent quadrants, as presented in Fig. 14. In this arrangement, the elements are mirrored repeatedly in both x and y directions. So that, each element is the immediate mirror of its neighbor elements in both x and y directions. In other words, the radiated fields of every two adjacent elements viewed as a pair, would eliminate the farfield cross-polar component. Fig. 15 presents the phase distribution obtained through the compensation phase formula and the feed height calculation. The phase distribution diagram also reveals a noticeable symmetric relationship in the compensation phase of the reflecting units on the reflectarray.

4. RESULTS AND DISCUSSION

To validate the design of the proposed reflectarray antenna, a prototype was constructed, as depicted in Fig. 16. The reflectarray was printed on the PTFE substrate, while a single-side etched substrate was utilized as the ground plane. The accurate formation of the air layer between the two substrates was en-

sured with the use of eight Nylon screws. The support frame for the feed source was constructed using FR-4 substrates while the feed patch antenna was directly etched onto the horizontal support substrate. The distance from the feed patch antenna to the upper-layer dielectric substrate is 79 mm. The radiation performance of the manufactured prototype was assessed within a microwave anechoic chamber. Fig. 17 displays the measurement system utilized, where the reflection coefficient of the prototype antenna was measured using an Agilent E8362B vector network analyzer, and the distance from the receiving horn to the reflecting array antenna is 1.5 meters.

In Fig. 18, a comparative analysis of the reflection coefficient curves between the measured and simulated results is presented. The measured impedance bandwidth is observed to be slightly higher than the simulated bandwidth, which is primarily attributed to the imprecise relative permittivity of the substrate material. It is noted that the -10 dB impedance bandwidth achieved from the measurements is 2.88% (5.84–6.01 GHz) and 2.98% (10.36–10.67 GHz) at 5.9 GHz and 10.4 GHz, respectively.

Figures 19 and 20 present the radiation patterns obtained from measurements and simulations at 5.9 GHz and 10.4 GHz. The main lobe regions of both the measured and simulated radi-

ation patterns exhibit a high degree of similarity, except for the H -plane pattern at 5.9 GHz, which may be attributed to manufacturing errors and misalignment during the measurement process. The cross-polarization and sidelobe levels are observed to be below -23 dB and -11 dB, respectively, at 5.9 GHz, while at 10.4 GHz they are found to be lower than -21 dB and -11 dB, respectively.

The present study presents a comprehensive analysis of the 1-dB gain bandwidths measured for the proposed antenna design, which are illustrated in Fig. 21. Specifically, the C-band and X-band exhibit narrow 1-dB gain bandwidths of 9.15% (5.83–6.37 GHz) and 3.27% (10.12–10.46 GHz), respectively. The simulation and measurement results confirm the dual-band radiation characteristics of the proposed antenna design. It is worth noting that the narrow gain bandwidths observed in the dual bands can be attributed to the relatively narrow band performance of the slotted rectangular-patch feed antenna employed in the design.

Table 3 presents a comparative analysis of the performance of the proposed dual-band reflectarray antenna with prior works. The results demonstrate that the proposed antenna offers a larger frequency ratio and wider phase shift range. As previously highlighted, the reflectarray antenna displays favorable radiation properties in both bandwidths.

5. CONCLUSION

This paper presents a low-profile and easy-to-manufacture single-layer reflectarray antenna for dual-band operation in C- and X-bands. The proposed design utilizes a square ring loaded with four two-segment delay lines for the C-band element and two square rings with varying lengths and widths for the X-band element. The achieved phase shift ranges are 375° to 560° at 5.9 GHz and 10.4 GHz, respectively, resulting in a larger frequency ratio of 1.76. The measured results of the proposed reflectarray antenna are in good agreement with the simulation, achieving a peak gain of 16.45 dBi at 6.2 GHz and 17.1 dBi at 10.3 GHz, with measured -10 dB impedance bandwidths of 2.88% (5.84–6.01 GHz) and 2.98% (10.36–10.67 GHz). The comparison with previous works indicates that the proposed antenna exhibits a larger frequency ratio and wider phase shift range. The superior radiation characteristics of the proposed reflectarray antenna offer valuable insights for the study of dual-band and multi-band operations.

ACKNOWLEDGEMENT

This work was supported by the National Natural Science Foundation of China (Grant 62071282), and by the Open Foundation of China-Belarus Belt and Road Joint Laboratory on Electromagnetic Environment Effect (Grant ZBKF2022020102).

REFERENCES

- [1] Rubio, A. J., A.-S. Kaddour, and V. Georgakopoulos, "A mechanically rollable reflectarray with beam-scanning capabilities," *IEEE Open Journal of Antennas and Propagation*, Vol. 3, 1180–1190, 2022.
- [2] Li, H., X. Qi, T. Zhou, Z. Xu, and T. A. Denidni, "Wideband reconfigurable reflectarray based on reflector-backed second-order bandpass frequency selective surface," *IEEE Transactions on Antennas and Propagation*, Vol. 70, No. 12, 12 334–12 339, Dec. 2022.
- [3] Wu, W., K.-D. Xu, Q. Chen, T. Tanaka, M. Kozai, and H. Minami, "A wideband reflectarray based on single-layer magneto-electric dipole elements with 1-bit switching mode," *IEEE Transactions on Antennas and Propagation*, Vol. 70, No. 12, 12 346–12 351, Dec. 2022.
- [4] Su, T., X. Yi, and B. Wu, "X/Ku dual-band single-layer reflectarray antenna," *IEEE Antennas and Wireless Propagation Letters*, Vol. 18, No. 2, 338–342, Feb. 2019.
- [5] Nayeri, P., F. Yang, and A. Z. Elsherbeni, *Reflectarray Antennas: Theory, Designs and Applications*, Wiley, New York, NY, USA, 2018.
- [6] Abdollahvand, M., K. Forooraghi, J. A. Encinar, Z. Atlasbaf, and E. Martinez-de Rioja, "A 20/30 GHz reflectarray backed by FSS for shared aperture Ku/Ka-band satellite communication antennas," *IEEE Antennas and Wireless Propagation Letters*, Vol. 19, No. 4, 566–570, Apr. 2020.
- [7] Xu, P., L. Li, R. Li, and H. Liu, "Dual-circularly polarized spin-decoupled reflectarray with FSS-back for independent operating at Ku-/Ka-bands," *IEEE Transactions on Antennas and Propagation*, Vol. 69, No. 10, 7041–7046, Oct. 2021.
- [8] Deng, R., F. Yang, S. Xu, and M. Li, "An FSS-backed 20/30-GHz dual-band circularly polarized reflectarray with suppressed mutual coupling and enhanced performance," *IEEE Transactions on Antennas and Propagation*, Vol. 65, No. 2, 926–931, Feb. 2017.
- [9] Li, W., Y. Wang, S. Sun, and X. Shi, "An FSS-backed reflection/transmission reconfigurable array antenna," *IEEE Access*, Vol. 8, 23 904–23 911, 2020.
- [10] Zhong, X., H.-X. Xu, L. Chen, W. Li, H. Wang, and X. Shi, "An FSS-backed broadband phase-shifting surface array with multi-mode operation," *IEEE Transactions on Antennas and Propagation*, Vol. 67, No. 9, 5974–5981, Sep. 2019.
- [11] Tahseen, M. M. and A. A. Kishk, "Flexible and portable textile-reflectarray backed by frequency selective surface," *IEEE Antennas and Wireless Propagation Letters*, Vol. 17, No. 1, 46–49, Jan. 2018.
- [12] Kong, G., X. Li, Q. Wang, and J. Zhang, "A dual-band circularly polarized elliptical patch reflectarray antenna for high-power microwave applications," *IEEE Access*, Vol. 9, 74 522–74 530, 2021.
- [13] Farias, R. L., C. Peixeiro, and M. V. T. Heckler, "Single-layer dual-band dual-circularly polarized reflectarray for space communication," *IEEE Transactions on Antennas and Propagation*, Vol. 70, No. 7, 5989–5994, Jul. 2022.
- [14] Thiruvoth, D. V., A. A. B. Raj, B. P. Kumar, V. S. Kumar, and R. D. Gupta, "Dual-band shared-aperture reflectarray antenna element at Ku-band for the TT&C application of a geostationary satellite," in *2019 4th International Conference on Recent Trends in Electronics, Information, Communication & Technology (RTEICT)*, 361–364, 2019.
- [15] Costanzo, S., F. Venneri, A. Borgia, and G. D. Massa, "Dual-band dual-linear polarization reflectarray for mmWaves/5G applications," *IEEE Access*, Vol. 8, 78 183–78 192, 2020.
- [16] Serup, D. E., G. F. Pedersen, and S. Zhang, "Dual-band shared aperture reflectarray and patch antenna array for S- and Ka-bands," *IEEE Transactions on Antennas and Propagation*, Vol. 70, No. 3, 2340–2345, Mar. 2022.